Energy absorption and collapse behavior of PP -based pin-reinforced composite sandwich panels under quasi-static flatwise compression loading

Pedram, E., Ahmadi, H., Kabiri, A., Choobar, M. G., Razmkhah, O., Fellows, N. & Liaghat, G.

DOI 10.1002/pc.27307
ISSN 0272-8397
ESSN 1548-0569

Publisher: Wiley

Received: 2 October 2022 | Revised: 23 February 2023 | Accepted: 24 February 2023

DOI: 10.1002/pc.27307

RESEARCH ARTICLE

Polymer COMPOSITES WILEY

Energy absorption and collapse behavior of PP-based pin-reinforced composite sandwich panels under quasi-static flatwise compression loading

Ehsan Pedram[1] | **Hamed Ahmadi**[2] | **Ali Kabiri**[2] | **Mehran Ghalami Choobar**[3] | **Omid Razmkhah**[4] | **Neil Fellows**[5] | **Gholamhossein Liaghat**[5]

[1]Faculty of Mechanical and Civil Engineering, Islamic Azad University, Qazvin, Iran

[2]Faculty of Mechanical Engineering, Tarbiat Modares University, Tehran, Iran

[3]Research and Development Department, Faravari and Sakht Co., Rasht, Iran

[4]School of Mechanical, Aerospace, and Automotive Engineering, Coventry University, Coventry, UK

[5]School of Engineering, Computing, and Mathematics, Faculty of Technology, Design, and Environment, Oxford Brookes University, Oxford, UK

Correspondence
Gholamhossein Liaghat, School of Engineering, Computing, and Mathematics, Faculty of Technology, Design, and Environment, Oxford Brookes University, Oxford, UK.
Email: gliaghat@brookes.ac.uk

Abstract

This article investigates the energy absorption and failure behavior of thermoplastic composite sandwich panels made entirely of polypropylene (PP) and pin-reinforced core under quasi-static compressive loading. The pins are manufactured by thermoforming and assembled with face sheets. The specimens were subjected to flatwise compressive loading to examine energy absorption capabilities. Moreover, the finite element method (FEM) is used to analyze core sandwich panels reinforced with cubic, cylindrical, beam, and cross-beam pins. Furthermore, a closed-form analytical model is adopted and developed to predict the critical load of these structures. The performed experiments were utilized to validate the damage mechanisms and critical displacements of the simulations and the analytically calculated maximum collapse loads. The results demonstrate that the predictions accurately capture both the critical failure load and failure mechanisms. Since the numerical results have a reasonable correlation with the experimental results and their output difference is <15%, FEM is used to investigate the collapse behavior of the pin-reinforced foam-filled panels. A comparison of the load–displacement, specific energy absorption (SEA), and maximum collapse loads of the samples shows that the cubic reinforced foam-core sandwich panel has the maximum peak load and SEA. The FE model of pin-reinforced foam-filled panels reveals that the buckling of the reinforcements is postponed to a point beyond the critical one. Hence, PP foam can act as lateral support and delay the ultimate failure in panels, especially pin-reinforced cylindrical sandwich panels, up to 40%.

KEYWORDS

composite sandwich panels, energy absorption, flatwise compression, pin-reinforcement, polypropylene

1 | INTRODUCTION

Composite sandwich structures are popular in various sectors, including automotive, aerospace, civil, and naval industries due to advantages, such as superior specific strength-to-weight ratio, stability, and ease of fabrication and repair.[1] The primary shortcoming of the thermoset polymer used in composite sandwich structures is non-recyclability.[2] Hence, thermoplastic polymer matrices have recently gained popularity over thermosets because of unique properties such as short production cycles, cheaper processing, and good reparability.[3] Thermoplastics soften when heated and are useful in processes where waste materials can be recycled, such as extrusion, injection molding, and hot-press molding. Therefore, composite sandwich structures based on specific thermoplastic polymers have been widely utilized, developed, and reported in the literature.[4,5] The most demanded thermoplastic polymers (90% of total demand) are five main commodity types, namely polyethylene (PE), polypropylene (PP), polyvinyl chloride (PVC), polyethylene terephthalate (PET), and polystyrene (PS).[6] PP has many advantages, including high-temperature resistance, low density, acceptable impact resistance, low water absorption, non-toxicity, transparency, dimensional stability, good fatigue resistance, and recyclability.[7] These benefits make PP suitable for numerous industrial products such as trays, funnels, pails, bottles, carboys plastic containers, cooler containers, insulation for electrical, stationery folders, water filters, and instruments that require frequent sterilization for the clinical setting and is very suitable for filling, reinforcing, and blending.[8]

Several analyses have been performed by modifying the composition of the polypropylene core to maintain the material characteristics for the skin and cohesive surfaces in every configuration. For instance, to compare the mechanical response of several sandwich panel configurations made by a polypropylene (PP) honeycomb core and carbon fiber reinforced polymer (CFRP) outer skins, Akanfora et al. performed experimental and numerical low-velocity impact analysis.[9] Furthermore, Daiyan et al. obtained the low-impact response of elastomer-modified polypropylene under different loading conditions and achieved their force–deflection curves and failure patterns.[10,11] The buckling performance of neat PP is acceptable; however, it has low compressive strength that can jeopardize its structural application and requires reinforcement to satisfy load-bearing applications. In the design of PP components, it is necessary to address this low compressive strength by reinforcing with fibers such as glass to withstand bending and compressive loads. Glass fibers have proper mechanical properties and reasonable cost, making them widespread materials in reinforcing PP.[5] Moreover, glass fibers are naturally hydrophobic and very stable compared with PP. It was demonstrated that PP and E-glass fibers have high fiber-matrix adhesion due to their hydrophobicity.[5,12] Recently, Kabiri et al. conducted a study on the mechanical behavior of PP/Glass plates for biological application through experiments on long unidirectional prepreg, short randomly oriented, and long unidirectional fiber yarn used as reinforcement.[13] In addition, they pointed out that the use of glass fiber improves the design aspects and mechanical properties of neat PP.[14,15]

In the literature, sandwich structures with traditional core arrangements such as cork,[16] honeycomb,[17] corrugated,[18] pyramid,[19] and rod[20] have mostly been studied, and sandwich structures with a foam core reinforced through-thickness struts have rarely been studied. Materials with reduced density are usually strengthened by suitable reinforcement elements, so they achieve a higher load-carrying capacity through the direction of thickness while maintaining the lightweight.[21] These reinforcing elements are classified into three categories. The first group is based on the matrix constituent.[22,23] The second category consists of reinforcing the foam core of the sandwich panel with fibers using different methods.[24] The final category is the particulate composite elements. Particulate core reinforcement includes reinforcement by 3D truss-like, pins, and many other shapes with approximately the same size and dimensions used between two face sheets.[25–29] In the most of reported data regarding the energy absorption in composite structures, circular and square cross-sections have been used. Moreover, there is a general agreement that energy absorption highly dependent on the geometry of the structure. In this regard, Hull proved that size and shape are among the five essential variables that affect the specific energy absorption in composite structures.[30] Abdi et al. reinforced foams with cylindrical polymer struts and observed a substantial increase in planar compression and flexural properties of sandwich panels.[31] They indicated that flexural stiffness is significantly affected by the diameter of the pins. Rafael Delucis et al. investigated polyethylene terephthalate foam core sandwich panels reinforced by transverse polymeric pins under flatwise compressive and flexural loading experimentally.[32] Furthermore, they found an acceptable correspondence through a numerical approach to a nonlinear crushable foam model and 3D elements for the pins.

Research on thermoplastic composite sandwich structures with pin-shaped particle reinforcement for specific applications is limited. With this in mind, this study reports the investigation of energy absorption capacity and damage identification of a new concept of a PP-based composite sandwich panel. Pin-reinforced composite

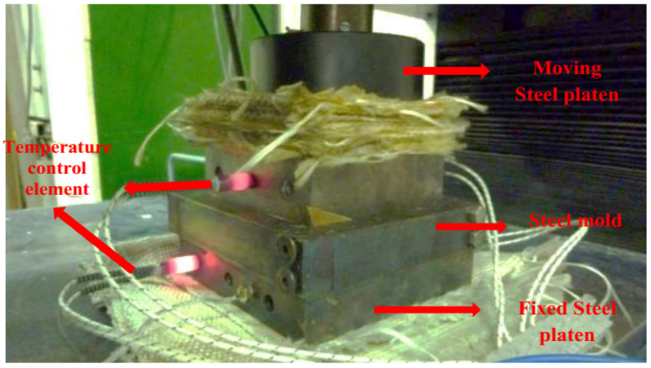

FIGURE 1 Specimen fabrication process utilizing thermoforming.

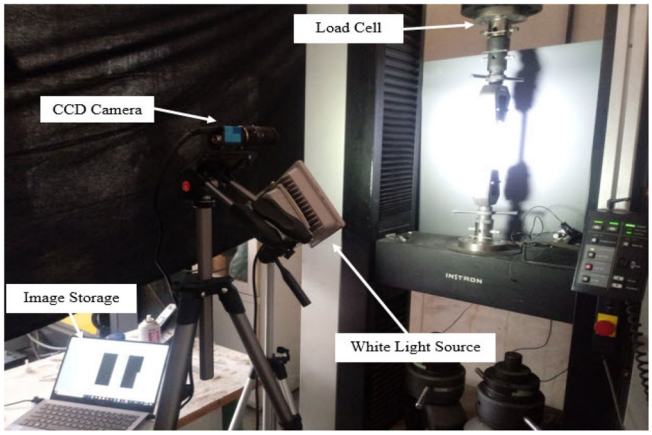

FIGURE 2 The tensile, compression, and in-plane shear tests setup.

sandwich panels (PRCSPs) were considered entirely of PP materials, with PP foam as core filler, neat PP as skins, and PP/Glass through-thicknesses reinforcement with particulate form elements. Using the thermoforming process, foamless panels were fabricated and then subjected to flatwise compression tests to evaluate their compression behaviors and damage mechanisms. Through a simple analytical formula based on Euler's theory, the prediction of pins collapse load was developed considering buckling and shear modes. A 3D finite element model of sample structures was generated using ANSYS software, which was validated through load–displacement diagrams of tested samples. Simulations were also used to study the load-bearing capacity, energy absorption, and deformation modes of conceptual foam core pin-reinforced composite sandwich panels.

2 | EXPERIMENTAL PROCEDURE

2.1 | Fabrication of specimens

In this study, face sheets and pins were produced from neat PP granules and PP/short chopped glass fiber granules with a volume fraction of 15%, respectively. Thermoforming is the process of pressing a deformable material, which is charged between two-heated molds under high mold temperature and transforming the material into a solid by cooling under pressure. This method is suitable for producing parts with high volume and low cost. To manufacture the specimen components, the granules were placed into the steel molds heated by heating elements to control the temperature during the compression process. Temperature, time, and pressure are the main parameters of the thermoplastic composite manufacturing process determined via the design of experiments (DOE). The mold was heated to a temperature of 200°C and a pressure of 1 MPa for 20 min. When the pressure is high, no void formation occurs and only a few imperfections remain in the finished product due to the handmade construction. The molding configuration is shown in Figure 1. The sheets were detached from the mold after the hot press cooled down to below 40°C. A visual examination, then, checked the defects and discontinuities.

2.2 | Microscopic investigation and physio-mechanical characterization of materials

The morphology of PP/short chopped glass fiber was inspected by scanning electron microscope (SEM) at room temperature. A few nanometers of thick gold was coated on the surface, and it was examined with a voltage of 5 kV in the secondary electron mode at 800 magnification.

Density (ASTM D792), tensile (ASTM D3039 and ASTM D638 (for neat PP)), compression (ISO 844), and in-plane shear (ASTM D3518) tests were conducted based on ASTM regulations to measure the mechanical and physical properties of neat PP and PP/Glass. The tensile, compression, and in-plane shear tests setup is shown in Figure 2. Tests were performed using a 5500 series universal test machine (Instron Co. UK) at room temperature. Digital image correlation (DIC) technique was used to acquire a precise strain field. For all tests, the experiments were repeated thrice to confirm the reliability of the results. Then, the mean and the standard deviation (SD) values were evaluated and reported.

2.3 | Conceptual PRCSPs design

The results of the previous section indicate that, although the modulus of the PP/Glass is considerably higher than

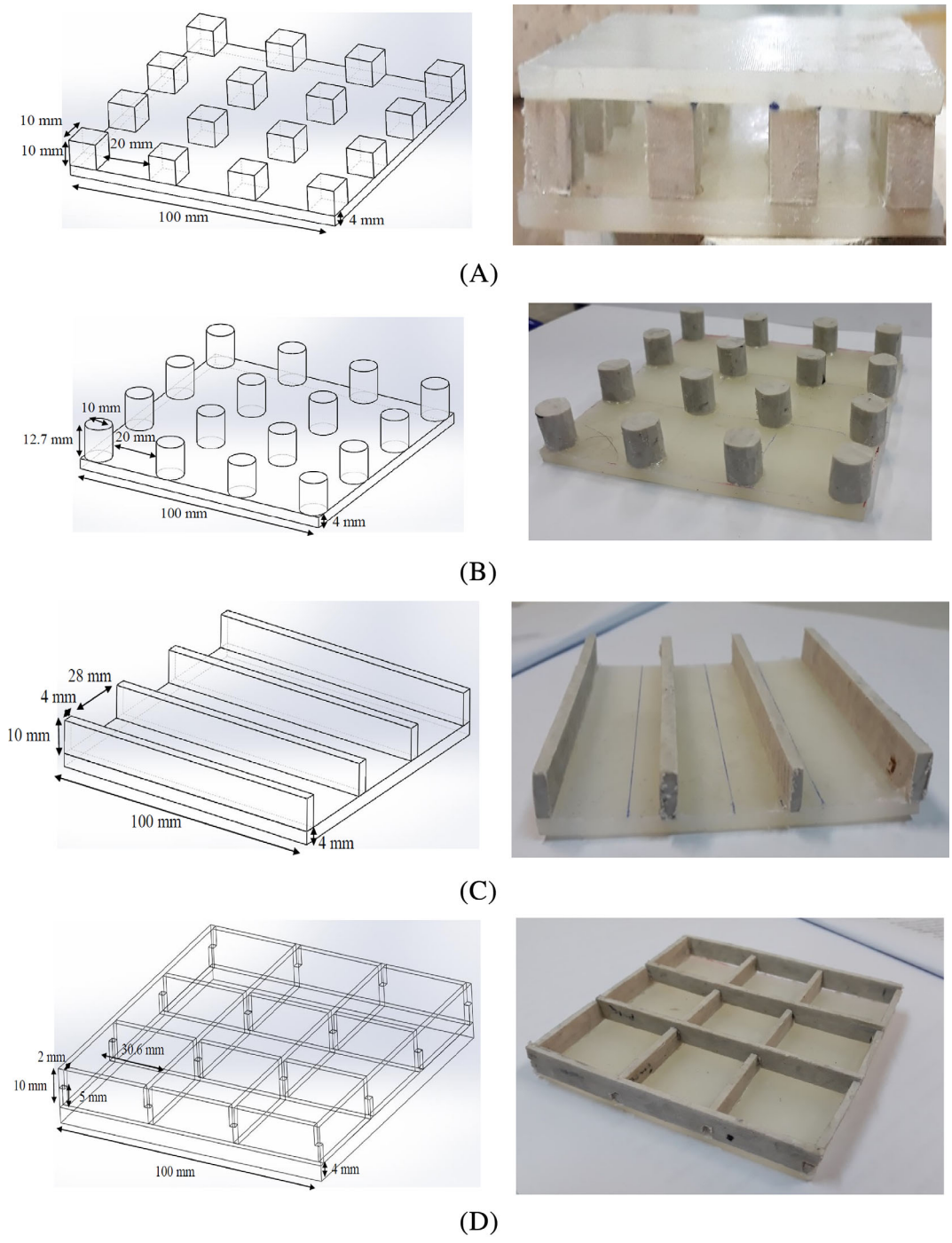

FIGURE 3 Sketch and geometrical values of different pins embedded between the panels face sheets; (A) cubic, (B) cylindrical, (C) beam, and (D) cross-beam.

neat PP, the neat PP is capable of weight-saving over PP/Glass for applications limited in stiffness. Therefore, to achieve a proper sample configuration with desirable properties, the neat PP face sheets and the PP/Glass pins were made. The equivalent volume fraction of different pin shapes was taken the same. The schematic concept of composite sandwich panels reinforced with particle pins consisting of cubic, cylindrical, beam, and cross-beam elements with specific dimensions is depicted in Figure 3. An epoxy adhesive (ML350) was used to assemble the components. It was applied to the pin joints and face sheets under a pressure of 0.1 MPa at room temperature until it meld. Then, sandwich panels were heated in

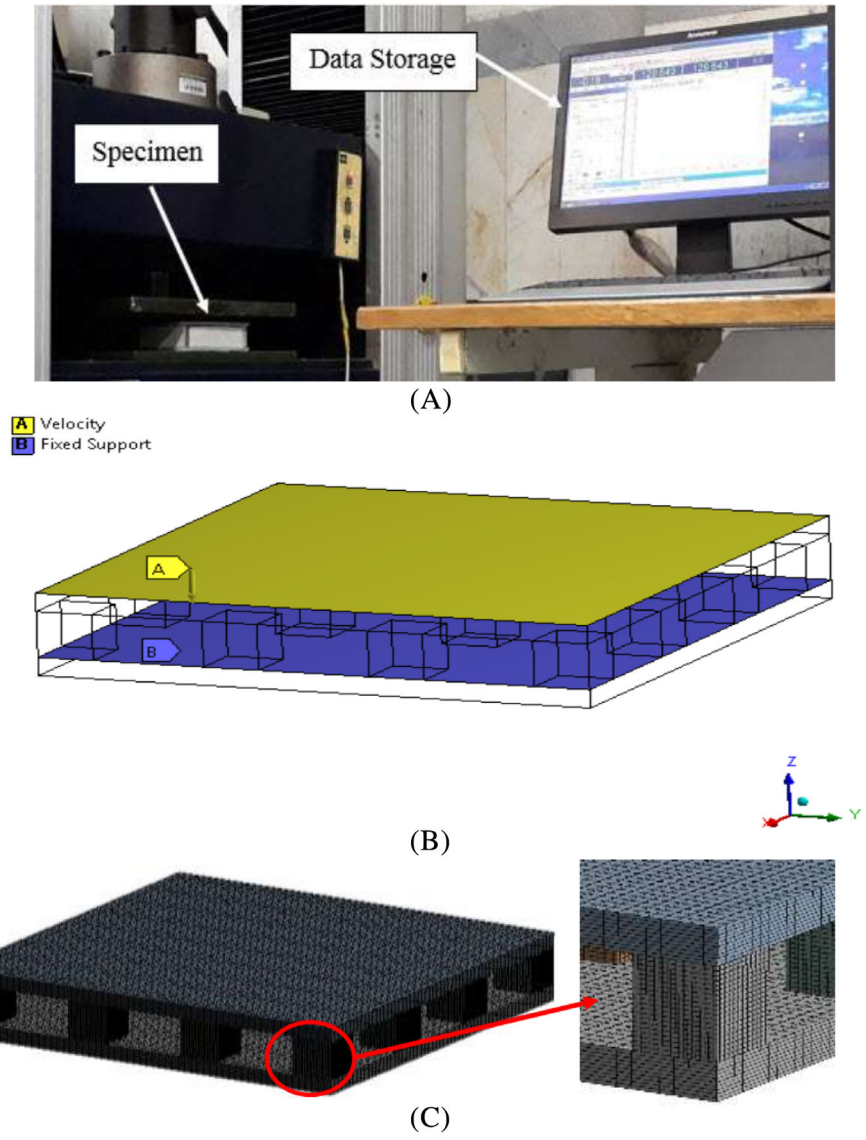

FIGURE 4 (A) Quasi-static compressive test setup, (B) schematic figure of the boundary conditions, and (C) FE mesh of the modeled cubic pin-reinforced sandwich panel.

an oven at 80°C for approximately 60 min to cure the adhesive.

2.4 | Flatwise-compressive loading

Quasi-static flatwise-compressive tests were performed by a universal test machine with a 300 kN load cell. Figure 4A shows the specimen mounted between two square steel plates with dimensions of 200 × 200 × 20 mm. The moving plate of the testing machine exerted uniform axial compression with a nominal displacement of 10 mm/min during the compression test. A nominal strain rate of $10^{-2}S^{-1}$ was employed in all tests. A load cell connected to data storage was used to evaluate the applied load. Each type of sample was tested at least three times. Load–displacement traces were recorded until the specimens lost their stability and were fully crushed.

3 | NUMERICAL INVESTIGATION

Numerical models were developed to simulate the compression response of the sandwich structures under quasi-static loading. The finite element (FE) model of PRCSPs was created using the finite element package of ANSYS Workbench 19.0 software (ANSYS Inc., Canonsburg, PA). The 3D geometry of the sandwich panels was modeled and assembled in Solid Works (Dassault Systems, MA), and then the models were imported into the ANSYS. The loading condition was exerted on the first layer of the frontal face sheet. The area under the lower layer was also used as boundary conditions in the *x*, *y*, and *z* directions. All translational degrees of freedom were restrained at the lower surface of the plate. The nodes on the frontal and distal surfaces were constrained completely, except for the upper surface nodes in the z-direction (Figure 4B).

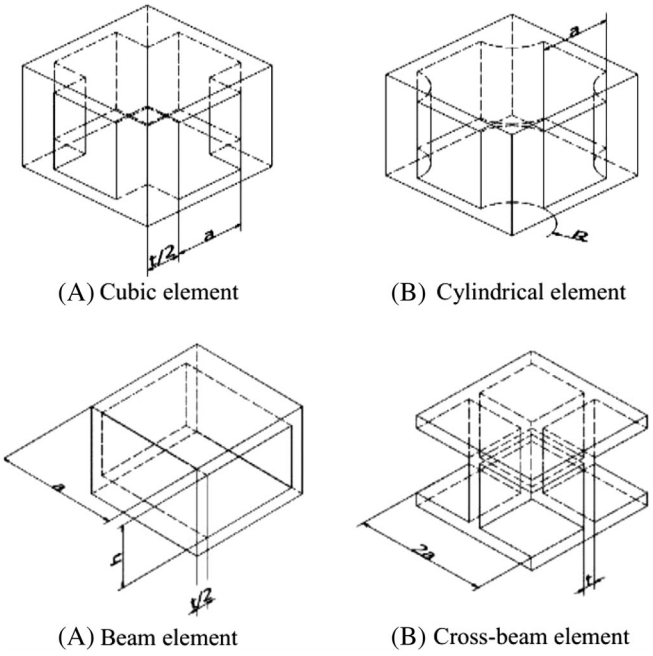

FIGURE 5 A unit element representing the through-thickness pins.

As shown in Figure 4C using the ANSYS element library, all parts were meshed by SOLID92 elements, including the quadratic displacement field, defined by 10 nodes with three-degree freedom at each node, translations in the nodal directions of x, y, and z. Almost 300,000 elements were used in this model. Explicit nonlinear numerical analyzes have been run on the ANSYS FEM code platform. ANSYS uses Newton's method to solve the nonlinear equilibrium equations, and the solution is obtained through a series of load increments. In the present solution, the default automatic incrimination scheme is used because it will select increment sizes based on computational efficiency.

3.1 | Contact elements and mesh convergence

The contact interfaces of the core and layers were used with surface-to-surface contact with penalty-based contact conditions at a frictional coefficient of 0.8 (based on recent studies[33]). In addition, nonlinear frictional contact (contact 49) was used to simulate an interfacial condition. In the modeling procedure, isotropic linear elastic and perfectly plastic behavior were defined to introduce the material model of neat PP and PP/Glass. The elastic–plastic behavior of the polymeric component has been considered in the framework of this study by implementing the true stress–strain law in accordance with the polymeric material properties (listed in Table 2), which considers both the elastic and plastic phases. In particular, the yield stress, Young's modulus, plastic deformation, and other properties of neat PP and PP/Glass were all obtained from the mechanical characterization tests, which provided all the material data through stress–strain curves. Fracture criterion (maximum principal stress criterion) and element removal algorithm were suggested for element deletion of structures.[34] Therefore, the maximum principal stress can be applied for a more realistic prediction of damage. This algorithm, by adopting a Continuum Damage Mechanics (CDM) based formulation, considers fibers and matrix damage mechanisms in tensile and compressive loading conditions. According to CDM, for each failure mode, two different phases are defined: a first phase, representing the linear mechanical behavior up to the damage onset threshold, and a second phase, representative of the damage evolution up to the complete failure. The response of the material after damage initiation, which describes the rate of degradation of the material stiffness once the initiation criterion is satisfied.

TABLE 1 Cross-section area, second moment of area, and gyration radius for the studied configurations.

	A (m^2)	I (m^4)	K (m)
Cylinder	$\frac{\pi}{4}D^2$	$\frac{\pi D^4}{64}+\frac{\pi D^2(a+2R)^2}{2}$	$\sqrt{\frac{D^2}{16}+\frac{a^2+D^2}{2}}$
Cubic	t^2	$\frac{t^4}{12}+2t^2\left(\frac{a}{2}+\frac{t}{2}\right)^2$	$\sqrt{\frac{t^2}{12}+\frac{a^2+t^2}{2}}$
Beam	$2\times\frac{t}{2}a$	$\frac{at^3}{12}+\frac{tab^2}{2}$	$\sqrt{\frac{t^2}{12}+\frac{b^2}{2}}$
Crossbeam	$4\times\frac{t}{2}a$	$\frac{at^3}{12}+\frac{ta^3}{2}$	$\sqrt{\frac{t^2}{24}+\frac{a^2}{4}}$

To verify the model, a convergence test was performed beforehand to ensure the convergence of the numerical model results. Mesh sensitivity was investigated by varying the mesh density within the plane and through-thickness directions. The convergence of strain energy and maximum values of von Mises stress were evaluated in all models. The tolerance level was a change of less than 5%, with approximately 300,000 elements. Therefore, according to the mesh sensitivity analysis, a size of 0.1 mm was chosen for the elements. Furthermore, the quality of the elements, which indicates the suitability of the element regarding the model geometry, was close to 1, the aspect ratio was from 0 to 1.2, and the Jacobin of the elements was 1. Considering all three indicators, good quality is possible for the selected elements in this analysis.

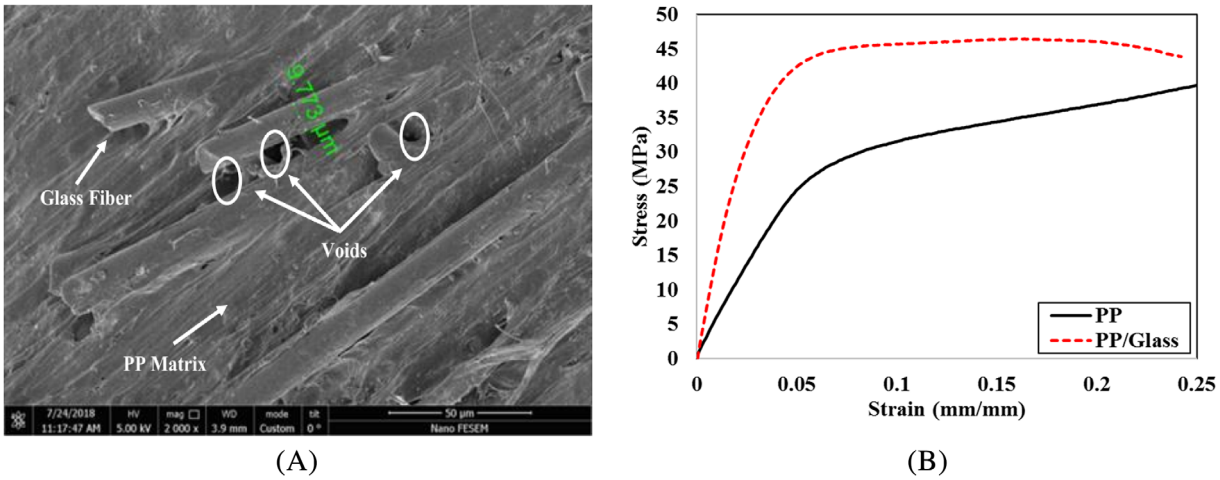

FIGURE 6 (A) SEM output showing the voids and fiber dispersion in PP matrix. (B) Achieved stress–strain curves of neat PP and PP/glass samples.

TABLE 2 Physical and mechanical properties of materials.

Materials	ρ (kg/m³)	*E* (GPa)	σ_T (MPa)	σ_C (MPa)	*G* (GPa)	τ (MPa)	ν
Neat PP	946 ± 5	0.77 ± 0.1	20 ± 5	30 ± 5	0.25 ± 0.1	10 ± 5	0.45 ± 0.05
PP/Glass	1040 ± 10	2.40 ± 0.15	30 ± 5	45 ± 5	0.80 + 0.1	20 ± 5	0.35 ± 0.05

3.2 | FE model of conceptual foam-filled pin-reinforced composite sandwich panel

In this study, finite element simulations were conducted to demonstrate the effect of PP foam fillers on the in-plane compression behavior of foam core PRCSPs. The main idea of combining the foam core with the pins is to reinforce the foam core to improve compression and shear performance, while the surrounding foam prevents pin buckling and helps transfer shear loads. The microstructure of the foam consists of micro-closed cells, which causes this specific stress–strain response to intense compression. At the plateau stress stage, heavy compressive strains are exerted on the foam, and it can absorb substantial specific energy.

The simulations were based on low-density (LD) and high-density (HD) PP thermoplastic foams reported by Bouix et al.[35] They tested a wide range of PP foam densities under quasi-static compression, and remarkably, the behavior of PP foams has three stages: (i) linear elastic behavior, (ii) plateau stress, and (iii) densification of foam. In this study, the plastic behavior was modeled using a crushable foam material model based on ANSYS user's manual recommendations. This model uses a volumetric hardening to simulate material in the plastic state. There are three surfaces; original surface, yield surface, and flow potential. From the numerical analysis, the load-displacement, specific absorbed energy, and induced damage mechanisms were extracted and compared with the cases without a foam filler.

4 | THEORETICAL MODELING

Figure 5 shows the assumed unit cell for modeling the four struts geometries inside the sandwich panels under flatwise compressive loading. The PP/Glass material is apparently ductile, and its behavior is almost fully plastic. Presuming rigid-perfect plastic behavior for PP/Glass under compression loading, the critical crushing load (P_{cr}) of the pin-reinforced sandwich panel is obtained as follows:

$$P_{cr} = J\, n\, \sigma_c A \tag{1}$$

Where σ_c, n and A represent the compressive strength of PP/Glass, the number of unit cells required to record the configuration, and the unit cells of the cross-sectional area, respectively. Furthermore, the J parameter incorporates the adhesive bonding efficiency in the model. It is assumed for pin and beams configurations 1 and 0.75, respectively.[36]

On the other hand, assuming an elastic behavior of the pin or beam elements, the critical buckling load (P_b) for the pin-reinforced sandwich panel can be calculated as:

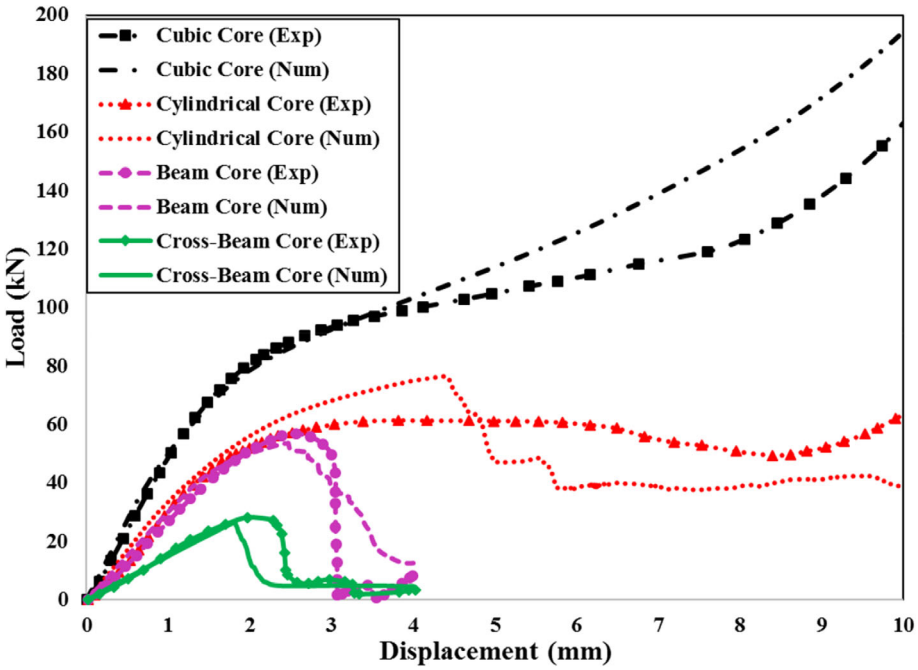

FIGURE 7 Comparison of experimentally and numerically load–displacement curves of sandwich structures.

Pin type	$H = H_F^* + H_P^{**}$	EXP (critical displacements) (mm)	NUM (critical displacements) (mm)
Cubic	8 + 10	4.5	4.7
Cylindrical	8 + 12.7	4.2	4.5
Beam	8 + 10	2.6	2.2
Crossbeam	8 + 10	2.3	1.9

TABLE 3 Comparison between critical displacements of samples.

Note: H_F^* = Face sheet thickness; H_P^{**} = Pin thickness.

$$P_b = \frac{\pi^2 D}{(kL)^2} \tag{2}$$

Which, $D = EI$ indicates the flexural modulus and L is the beam height. Furthermore, the k parameter indicates boundary conditions in the model, which considered 1 and 2 for simply supported (S-S) and clamped (C-C) end conditions, respectively (Table 1). The faceplates are not directly taken into account in the model, but their presence is considered through the applied boundary conditions to the struts. Then, the faceplates are assumed stiff enough; thereby they do not deform during compressive loading and do not affect the buckling behavior of the entire structure. In the planar compression test, the faceplates do not carry a noteworthy load; therefore, it is adequate to model the cores without face skins, while applying suitable boundary conditions.

In order to estimate the collapse loading of PRCSPs, the mentioned failure modes are combined together to construct a model simulating the hybrid behavior of the studied structures. Based on the empirical formula suggested by Rankine[37] the collapse load (P_c) can be estimated as follows:

$$\frac{1}{P_c} = \frac{1}{P_{cr}} + \frac{1}{P_b} \tag{3}$$

By substituting, the critical loads related to the crushing failure mode and that of the buckling phenomenon into above equation:

$$P_c = \frac{Jn\sigma_c A}{1 + \frac{Jn\sigma_c A(kL)^2}{\pi^2 D}} \tag{4}$$

An alternative approximate formula can be achieved by incorporating the shear deformation into Euler's buckling formula, Equation 4, as follows:

$$P_c = \frac{P_{cr}}{1 + \frac{P_{cr} 2(1+\upsilon)}{EA}} \tag{5}$$

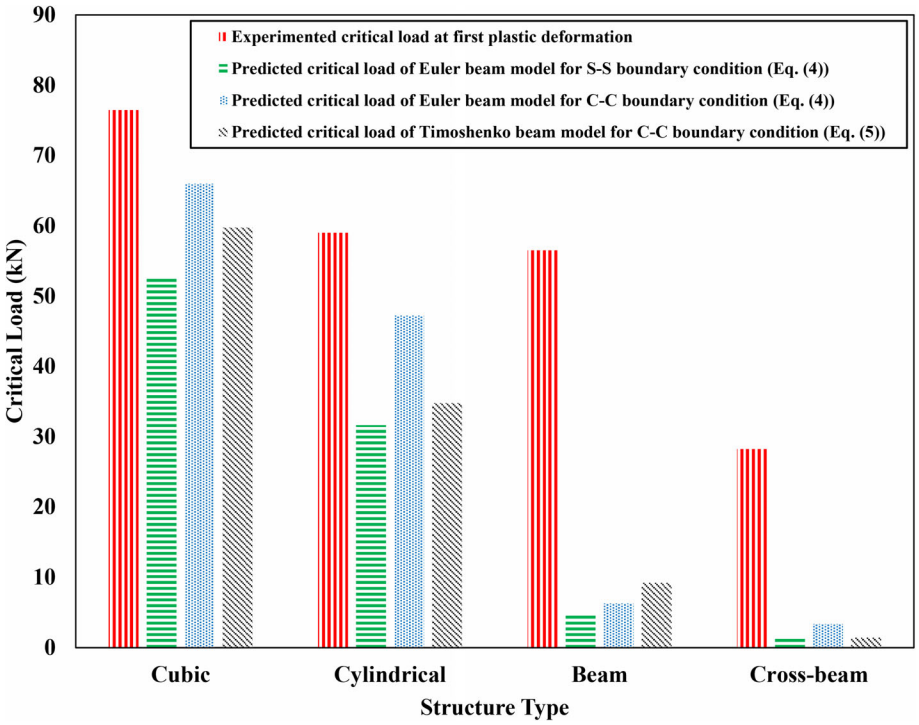

FIGURE 8 Comparison of obtained collapsing load of the proposed analytical model and experiments.

where υ denotes the Poisson's ratio of the utilized material.

5 | RESULTS AND DISCUSSION

5.1 | SEM and physio-mechanical properties of materials results

As Figure 6A shows, SEM was used to ensure the uniform dispersion of fibers in the thermoplastic PP matrix. As seen in the SEM micrograph, there is a thin covering layer of the PP matrix on the surface of the fibers, which likely improves the stress transfer capability. As thermoplastic polymers have a high viscosity, there are gaps and voids around the fibers (between the polymer matrix and the fibers) leading to the presence of some voids in the products. The fiber diameter was approximately 10 μm. The cross-section revealed that most of the chopped glass fibers were parallel.

The compression test results were recorded and plotted as a stress–strain curve to calculate the mechanical properties of the constituent materials (Figure 6B). To obtain the modulus of elasticity (i.e., the slope of the curve), linear regression was used in the linear domain of the experimental stress–strain curve. Table 2 depicts the mechanical and physical properties of incorporated materials.

5.2 | FEM validation

Experiments were performed to validate the load–displacement curves obtained from the numerical models. As shown in Figure 7, the load–displacement curves of different PRFCPs obtained from experimental tests and those of numerical simulations are compared. The initial section of the obtained response curves is quasi-linear due to the elastic behavior. Table 3 compares the critical displacement of the elastic compressive strength for all the sandwich panels. The maximum and minimum values are (4.2 and 4.8 mm) for the cylindrical pin and (2.3 and 1.9 mm) for the cross-beam pin, respectively. The slight difference between the numerical and experimental load-deformation diagrams is due to imperfections in the geometry, particularly the shape of pins. In addition, the pin buckling phenomenon contributes to the imperfect sensitivity of the results. Since the numerical results had a reasonable correlation with the experimental results, and their output difference is less than 15%, it was employed to investigate the collapse behavior of pin-reinforced foam-filled panels and the deformation mode analysis.

The numerical and experimental load–displacement curves are compared to study post-buckling behavior (Figure 7). The recorded curves of flatwise-compressive loading can be categorized into two distinct scenarios. The first scenario highlights three regions for pin-reinforced

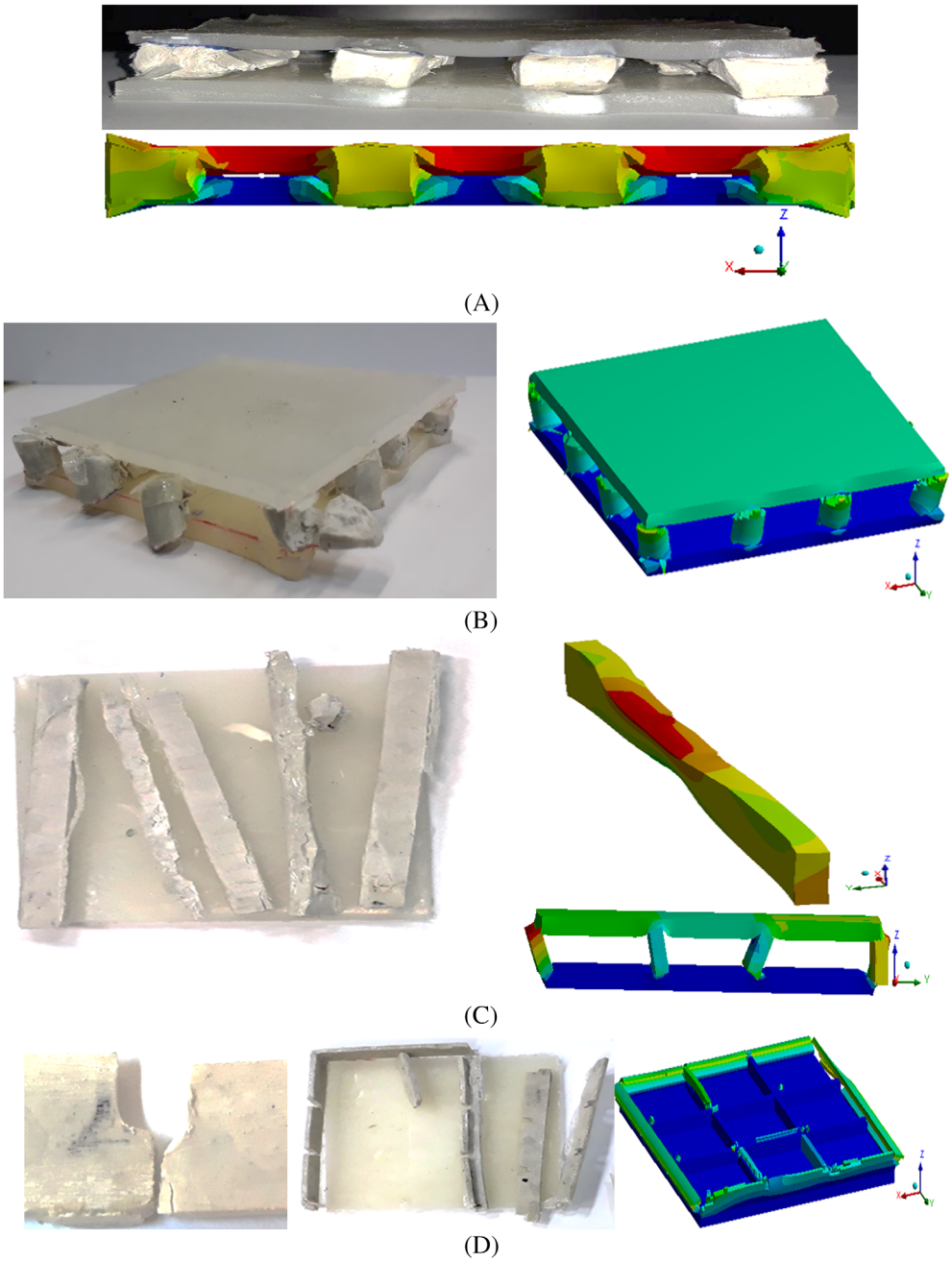

FIGURE 9 Damage mechanisms of (A) cubic pin-reinforced sandwich panel, (B) cylindrical pin-reinforced sandwich panel, (C) beam pin-reinforced sandwich panel, and (D) cross-beam pin-reinforced sandwich panel.

cubic and cylindrical pin-reinforced panels. The first region consists of the linear increase of the load up to a specific peak load. At this point, the pins lose their stability due to the initiation of plastic deformation. The second region (plateau) includes the curve, as the load remains persistent due to the collapse of the pins following plastic yielding. It seems that at this plateau, the properties of the pin cores under compression can be estimated by an elastic perfectly plastic material. In the third region, the load rises because of densification and plastic buckling of the pins. The figure shows that the densification phenomenon starts at a larger force for cubic struts than cylindrical ones. The higher stability of the cubic pins is the cause of the symmetric geometry and more contact surface with the face sheets and lower height. The second scenario belongs to the beam and cross-beam reinforcements. Raising the diagram is almost linear up to the first peak load, and then dropping is happened by beams collapsing due to the instability and consequently lateral movement of them. This trend for cross-beam reinforcements is catastrophic because the contact area beams with the face sheets reduce abruptly and shear stress increases in the cross slots of the longitudinal and transverse beams. The above-mentioned shear failure mode along with the buckling mode is responsible for

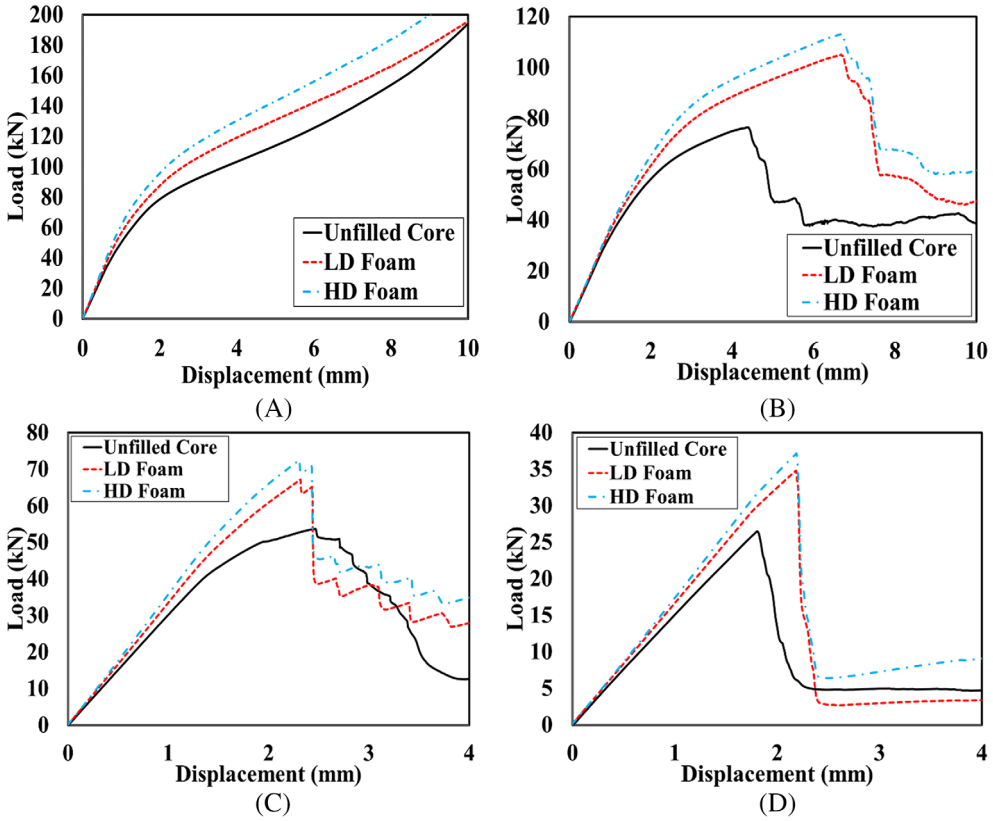

FIGURE 10 Comparison of load–displacement diagrams of sandwich structures with and without foam filling for (A) cubic, (B) cylindrical, (C) beam, and (D) cross-beam pin elements.

TABLE 4 Comparison of specific absorbed energy (SAE) of different core structures.

Pin type	Core type	Weight (kg) (±0.001)	AE (kJ)	SAE (kJ/kg)	SAE increase (%)
Cubic	Unfilled	0.092	1.128	12.260	–
	LD foam	0.097	1.243	12.814	4.514
	HD foam	0.107	1.368	12.785	4.275
Cylinder	Unfilled	0.092	0.460	5.000	–
	LD foam	0.098	0.689	7.030	40.612
	HD foam	0.110	0.756	6.872	37.454
Beam	Unfilled	0.094	0.130	1.382	–
	LD foam	0.097	0.145	1.494	8.088
	HD foam	0.107	0.162	1.514	9.475
Cross-beam	Unfilled	0.094	0.039	0.414	–
	LD foam	0.097	0.047	0.484	16.875
	HD foam	0.106	0.057	0.537	29.608

the collapse of the cross beam prior to the utilization of beam reinforcements capabilities.

5.3 | Analytical model results

The developed analytical model was used to predict the load corresponding to the first plastic deformation of the studied configurations. The comparison between the predictions of the proposed model, the Timoshenko shear deformation beam model, and those of the experimental tests is shown in Figure 8. The analytical solution shows a reasonable agreement between the predicted collapse loads of the experimental tests and the proposed equations for simply supported (S-S) and clamped (C-C) conditions. It should be mentioned that the prediction of

load is obviously smaller than that of the experimental. It was mainly due to that, the present analytical model was inaccurate for the large deformation in the densification process. Moreover, due to the decrease of a cross-section of columns in cross-beam pin-reinforced panels compared to cubic, cylindrical, and beam ones, the overall critical collapse load was significantly decreased. Actually, the average critical collapse load and the cross-section area slightly decrease with the slenderness.

5.4 | Damage characterization

Each test was terminated after the drop in load, and the specimens were then visually examined to determine the collapse mechanism. Failure mechanisms of the experimentally tested specimens and the FE model predictions are summarized into three collapse mechanisms: (i) elastic buckling of the pins, (ii) shear collapse of the pins, and (iii) plastic micro buckling of the face sheets. Figure 9A,B illustrate the post-crushing of cubic and cylindrical pin-reinforced panels compared to the simulation outputs. The numerical model successfully predicted the local buckling and sliding of the pins. Another failure mechanism in the sandwich panels with cubic and cylindrical pins that could be observed in both numerical and experimental tests is the localized crushed area of face sheet in the pin joint regions. Figure 9C,D show the deformation modes and failure mechanisms in the numerical simulations and experimental tests of the sandwich panels reinforced with beam and cross-beam. Local splitting damage at pin joining regions was identified as the primary failure mechanism in the sandwich panels. Indeed, the utilized numerical model correctly predict the lateral sliding and shear collapse of reinforcing elements of studied sandwiches under through-thickness compression. Lateral instability, specifically peripheral beams, is slightly more than that of cubic and cylindrical reinforcements.

5.5 | Foam-filling effects

In order to analyze the effects of foam filler on the load–displacement curves and consequently on the energy absorption behavior of sandwich structures, two cases consisting of low and high-density PP foams as core filler were considered. Figure 10 displays the load–displacement response of the specimens under planar compressive loading for different reinforcements. The first part of the curves was relatively linear in the elastic region, followed by the plastic region where the stress was almost constant under increasing deformation, and was produced by the development of localized buckling within the foam cell walls. After reaching the peak load, the struts in the core were partially buckled and, as a result, the overall stiffness of the specimen decreased. The load required to further deform the sample gradually decreases due to the propagation of localized buckling across the width of the core of beam and cross-beam structures. After that, a sudden drop in the applied load is happened to indicate that the structures lose stability due to plastic buckling. In fact, the figure shows that the linear region of curves is similar and the foam contribution is negligible. However, beyond the elastic region, the foam filler significantly enhances the curve of all structures, cylindrical and cubic ones (Table 4). It can be attributed that the foam core is the

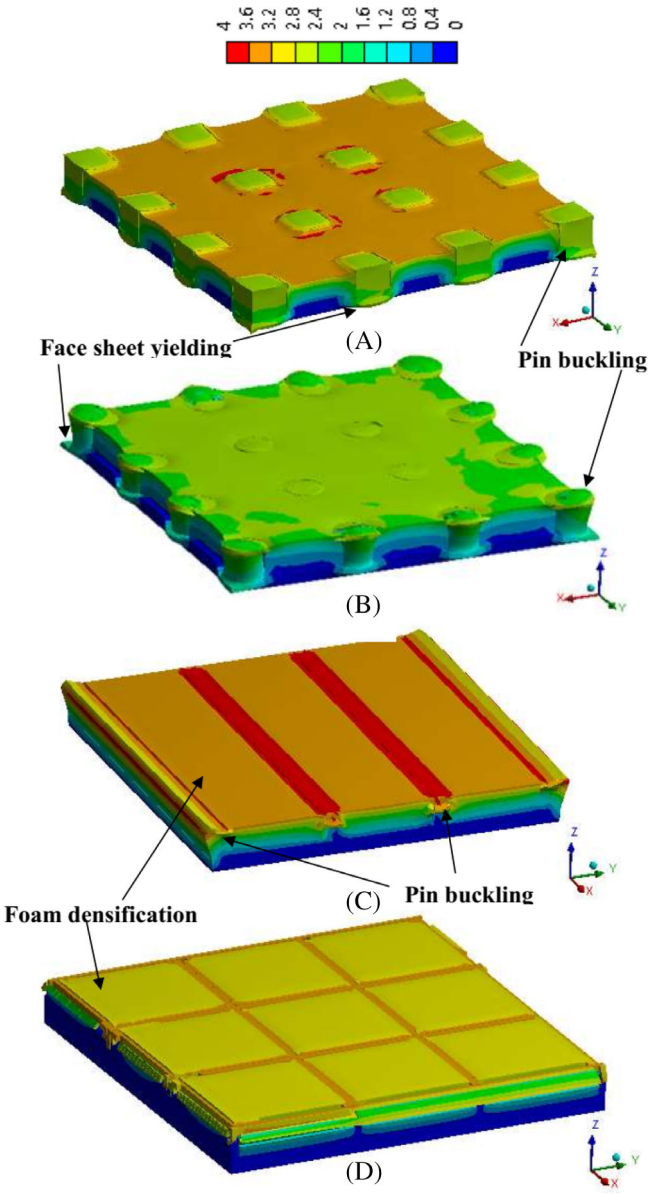

FIGURE 11 Deformation after crushing of pin-reinforced sandwich panels filled with foam.

dominant load-bearing material. The local contribution of the PP foam on the pins helps avoid premature buckling and increases energy increases on. Accordingly, the foam-filled cylindrical pin-reinforced sandwich panels have considerably more considered, compared to the unfilled one.

Figure 11 shows the failure mode of the different reinforcements of the studied sandwich panel. The figure shows that the foam directly improves the crushing capacity of the core, provides lateral support to the core struts, and supports their lateral movement while buckling. Furthermore, as can be seen from the comparison in terms of core ductility, the distribution of plastic area for the various configurations seems to be very similar. This behavior confirms that, at this energy level, the energy is mainly dissipated as fiber and matrix failures in the composite components. It should be noted that the use of foams in cores depends on their multifunctional advantages, including acoustic or thermal insulation and isolation of core spaces from the environment.

5.6 | Specific energy absorption

The energy absorption ability of panels could be evaluated using the flat-wise compression behavior. The energy absorption capacity (W) is obtained by integrating the stress–strain curve as follows:

$$W = \int_0^{\varepsilon_D} \sigma(\varepsilon) d\varepsilon \tag{6}$$

In this equation, $\sigma(\varepsilon)$ represents the compressive stress, ε represents the compressive strain when ε_D is the strain at the beginning of densification. The efficiency of the pin-reinforced panels is evaluated by calculating the Specific Energy Absorbed (SEA) of the samples per unit mass based on the D7336 standard.

Table 4 demonstrates the results of SEA calculations and the comparison of different reinforcements. Table 4 shows the significant contribution of foam filler on SEA of cylindrical and cross-beam reinforcement. In fact, foam filling results in the limited lateral movement of reinforcements and enhancement of pins stability and energy absorption.

6 | CONCLUSION

The present study was conducted to investigate the collapse behavior and energy absorption of PP-based pin-reinforced composite sandwich panels. Special attention was paid to investigating the effect of the simple shape of pin elements on load transfer and specific energy absorption of panels with and without foam filler. A finite element model was utilized to simulate the behavior of the panels and consequently to study the deformation modes and capture the damage mechanisms during compressive loading. A simple analytical approach was improved and employed to obtain the collapse loads of the panels and compared with those of experiments and showed the successful prediction of the collapsing load of pin-reinforced panels without foam filling material. The failure of the composite sandwich panels is generated by the phenomenon of pin buckling along with the shear collapse, especially for beam and cross-beam elements. The FE modeling of foam-filled pin-reinforced panels clarifies that the buckling of the reinforcement is postponed to a point beyond the critical one because of lateral support of the PP foam and the stability of the whole structure under compression. Furthermore, under compression, local buckling of the pins along with pin sliding because of plastic deformation of the face sheets is the first phenomenon of collapsing. As another result, although reinforcing the panels slightly increases the weight of the panels, the advancement in the flatwise compression performance is much pronounced. The experiments on the proposed composite sandwich panels with PP skins and PP/Glass pins show that a 3D thermoplastic composite core can create a successful combination with the PP surface in a quick and simple process.

DATA AVAILABILITY STATEMENT

The data that support the findings of this study are available from the corresponding author upon reasonable request.

ORCID

Hamed Ahmadi https://orcid.org/0000-0003-3869-4012
Gholamhossein Liaghat https://orcid.org/0000-0003-1925-0643

REFERENCES

[1] B. Abdi, S. Azwan, M. R. Abdullah, A. Ayob, Y. Yahya, *Polym. Compos.* **2016**, *37*(2), 612.
[2] N. K. Chandrasekaran, V. Arunachalam, *Polym. Compos.* **2021**, *42*(10), 5011.
[3] T. Khan, V. Acar, M. R. Aydin, B. Hülagü, H. Akbulut, M. Ö. Seydibeyoğlu, *Polym. Compos.* **2020**, *41*(6), 2355.
[4] G. Kumar, K. Ramani, C. Xu, *Polym. Compos.* **2002**, *23*(4), 647.
[5] Q. T. Shubhra, A. M. Alam, M. A. Quaiyyum, *J. Thermoplast. Compos. Mater.* **2013**, *26*(3), 362.
[6] H. A. Maddah, *Am. J. Polym. Sci.* **2016**, *6*(1), 1.
[7] A. L. Andrady, M. A. Neal, *Philos. Trans. R. Soc. B* **2009**, *364*(1526), 1977.
[8] S. K. Gulrez, M. E. Ali Mohsin, H. Shaikh, A. Anis, A. M. Pulose, M. K. Yadav, et al., *Polym. Compos.* **2014**, *35*(5), 900.
[9] V. Acanfora, M. Zarrelli, A. Riccio, *Int. J. Impact Eng.* **2022**, *171*, 104392.

[10] H. Daiyan, E. Andreassen, F. Grytten, O. V. Lyngstad, T. Luksepp, H. Osnes, *Polym. Test.* **2010**, *29*(6), 648.
[11] H. Daiyan, E. Andreassen, F. Grytten, O. V. Lyngstad, T. Luksepp, H. Osnes, *Polym. Test.* **2010**, *29*(7), 894.
[12] R. A. Khan, M. A. Khan, H. U. Zaman, S. Pervin, N. Khan, S. Sultana, A. I. Mustafa, *J. Reinf. Plast. Compos.* **2010**, *29*(7), 1078.
[13] A. Kabiri, G. Liaghat, F. Alavi, H. Saidpour, S. K. Hedayati, M. Ansari, M. Chizari, *J. Compos. Mater.* **2020**, *54*(30), 4903.
[14] A. Kabiri, G. Liaghat, F. Alavi, M. Ansari, S. K. Hedayati, *Proc. Inst. Mech. Eng. Part H: J. Eng. Med.* **2021**, *235*(12), 1439.
[15] A. Kabiri, G. Liaghat, F. Alavi, *Comput. Biol. Med.* **2021**, *132*, 104303.
[16] H. Kiratisaevee, W. J. Cantwell, *Polym. Compos.* **2004**, *25*(5), 499.
[17] Y. Mohamadi, H. Ahmadi, O. Razmkhah, G. Liaghat, *Thin-Walled Struct.* **2021**, *164*, 107785.
[18] S. A. Taghizadeh, A. Farrokhabadi, G. Liaghat, E. Pedram, H. Malekinejad, S. F. Mohammadi, H. Ahmadi, *Thin-Walled Struct.* **2019**, *135*, 160.
[19] J. Xiong, L. Ma, L. Wu, J. Liu, A. Vaziri, *Compos. Part B* **2011**, *42*(4), 938.
[20] J. Zhou, Z. W. Guan, W. J. Cantwell, *Polym. Compos.* **2017**, *38*(10), 2301.
[21] Z. Wang, Q. Chen, R. Du, T. Linghu, Y. Gao, G. Zhao, *Polym. Compos.* **2019**, *40*(S1), 449.
[22] S. Karkoodi, G. Liaghat, H. Z. Hosseinabadi, H. Ahmadi, *Wood Mater. Sci.Eng.* **2021**, *16*(6), 380.
[23] H. Ahmadi, G. H. Liaghat, M. M. Shokrieh, H. Hadavinia, A. Ordys, A. Aboutorabi, *J. Compos. Mater.* **2015**, *49*(10), 1255.
[24] F. Han, Y. Yan, J. Ma, *Polym. Compos.* **2018**, *39*(3), 624.
[25] A. Eyvazian, S. A. Taghizadeh, A. M. Hamouda, F. Tarlochan, M. Moeinifard, M. Gobbi, *J. Sandwich Struct. Mater.* **2021**, *23*(7), 2643.
[26] A. Henao, M. Carrera, A. Miravete, L. Castejón, *Compos. Struct.* **2010**, *92*(9), 2052.
[27] H. E. Yalkin, B. M. Icten, T. Alpyildiz, *Compos. Part B* **2015**, *79*, 383.
[28] T. Liu, Z. C. Deng, T. J. Lu, *Int. J. Solids Struct.* **2008**, *45*(18–19), 5127.
[29] M. Zupan, C. Chen, N. A. Fleck, *Int. J. Mech. Sci.* **2003**, *45*(5), 851.
[30] D. Hull, *Compos. Sci. Technol.* **1991**, *40*(4), 377.
[31] B. Abdi, S. Azwan, M. R. Abdullah, A. Ayob, Y. Yahya, L. Xin, *Int. J. Mech. Sci.* **2014**, *88*, 138.
[32] R. D. A. Delucis, M. L. P. Tonatto, R. S. Trindade, S. C. Amico, *J. Sandwich Struct. Mater.* **2021**, *23*(1), 241.
[33] Q. M. Li, R. A. W. Mines, *Int J. Exp. Mech.* **2002**, *38*(4), 132.
[34] C. E. Quenneville, C. E. Dunning, *Comput. Methods Biomech. Biomed. Eng.* **2011**, *14*(2), 205.
[35] R. Bouix, P. Viot, J. L. Lataillade, *Int. J. Impact Eng.* **2009**, *36*(2), 329.
[36] P. Le Grognec, *Thin-Walled Struct.* **2009**, *47*(8–9), 879.
[37] U. C. Jindal, *Machine design*, Pearson Education India, Delhi **2010**.

How to cite this article: E. Pedram, H. Ahmadi, A. Kabiri, M. G. Choobar, O. Razmkhah, N. Fellows, G. Liaghat, *Polym. Compos.* **2023**, 1. https://doi.org/10.1002/pc.27307